ATHEROSCLEROSIS

Copyright © 2020 The Authors, some rights reserved; exclusive licensee American Association for the Advancement of Science. No claim to original U.S. Government Works

siRNA nanoparticles targeting CaMKIIγ in lesional macrophages improve atherosclerotic plaque stability in mice

Wei Tao[1]*, Arif Yurdagul Jr.[2]*, Na Kong[1], Wenliang Li[1], Xiaobo Wang[2], Amanda C. Doran[2†‡§], Chan Feng[1], Junqing Wang[1], Mohammad Ariful Islam[1‖], Omid C. Farokhzad[1¶], Ira Tabas[2,3,4¶], Jinjun Shi[1¶]

Atherosclerotic lesional macrophages express molecules that promote plaque progression, but lack of mechanisms to therapeutically target these molecules represents a major gap in translational cardiovascular research. Here, we tested the efficacy of a small interfering RNA (siRNA) nanoparticle (NP) platform targeting a plaque-destabilizing macrophage molecule—Ca^{2+}/calmodulin-dependent protein kinase γ (CaMKIIγ). CaMKIIγ becomes activated in advanced human and mouse plaque macrophages and drives plaque necrosis by suppressing the expression of the efferocytosis receptor MerTK. When macrophage-targeted siCamk2g NPs were administered to Western diet–fed *Ldlr*$^{-/-}$ mice, the atherosclerotic lesions showed decreased CaMKIIγ and increased MerTK expression in macrophages, improved phagocytosis of apoptotic cells (efferocytosis), decreased necrotic core area, and increased fibrous cap thickness—all signs of increased plaque stability—compared with mice treated with control siRNA NPs. These findings demonstrate that atherosclerosis-promoting genes in plaque macrophages can be targeted with siRNA NPs in a preclinical model of advanced atherosclerosis.

INTRODUCTION

The activation of specific signaling pathways in macrophages can contribute to various disease processes. This scenario is particularly relevant to atherosclerosis, a disease characterized by arterial plaque deposition that gives rise to cardiovascular disease and stroke (*1*). For this reason, investigators have long considered ways to inhibit pro-atherogenic macrophage pathways to combat atherosclerotic vascular disease. Unfortunately, problems with specificity and efficacy have hindered this effort for many years.

RNA interference (RNAi) is a robust strategy to specifically inhibit or silence intractable therapeutic targets (*2*, *3*). A myriad of nanoparticle (NP) platforms have been developed for systemic delivery of RNAi therapeutics, including small interfering RNA (siRNA). These platforms have shown great promise in circumventing delivery barriers such as rapid blood clearance, nuclease degradation, low accumulation in diseased sites, and insufficient endosomal escape of siRNA to the cytoplasm. Several NP-based siRNA delivery platforms have been explored in clinical trials for different diseases, such as cancer, genetic disorders, hypercholesterolemia, fibrosis, and viral infections (*4*), with many more currently in preclinical phases (*5*). Notably, the first siRNA nanotherapeutic was recently approved by the U.S. Food and Drug Administration (FDA) for the treatment of a rare genetic disorder (*6*). Although several siRNA delivery platforms have been proposed for the treatment of vascular diseases (*7*–*11*), their use to specifically target macrophages in atherosclerotic lesions remains untested.

Here, we provide proof-of-principle evidence for the design and preclinical use of targeted siRNA NPs directed against the macrophage gene *Camk2g*, which encodes a calcium-activated kinase called CaMKIIγ (Ca^{2+}/calmodulin-dependent protein kinase γ). We chose this target because previous work established that lesional macrophage CaMKIIγ is activated in advanced human and mouse atherosclerotic plaques, where it promotes the conversion of relatively benign, fibrous atherosclerotic lesions into necrotic lesions with thin fibrous caps (*12*). Thin-capped, necrotic lesions represent the type of vulnerable plaques in humans that can precipitate plaque rupture, acute luminal thrombosis, and acute atherothrombotic vascular events, including myocardial infarction, unstable angina, sudden coronary death, and stroke (*13*). The mechanism involves CaMKIIγ-mediated interruption of a protective activating transcription factor 6 (ATF6)/liver X receptor alpha (LXRα)/c-Mer proto-oncogene tyrosine kinase (MerTK) pathway that normally functions to clear dead cells in lesions through a phagocytic process known as efferocytosis (*12*). Defective efferocytosis results in secondary necrosis of the uncleared cells and, ultimately, plaque necrosis, heightened plaque inflammation, and fibrous cap thinning.

We constructed NPs from poly(lactic-*co*-glycolic) acid (PLGA) polymer to load the siRNA/cationic lipid complex and from lipid–polyethylene glycol (lipid-PEG) to enable long-term circulation (*14*, *15*). In addition, a peptide called S2P, which recognizes the macrophage receptor stabilin-2 (*16*–*18*), was conjugated to the lipid-PEG layer on the NP surface to promote macrophage targeting. Our results demonstrate that treatment of fat-fed *Ldlr*$^{-/-}$ mice with established atherosclerosis with S2P-siCamk2g NPs silences lesional macrophage CaMKIIγ and promotes efferocytosis, increases fibrous

[1]Center for Nanomedicine and Department of Anesthesiology, Brigham and Women's Hospital, Harvard Medical School, Boston, MA 02115, USA. [2]Department of Medicine, Columbia University Irving Medical Center, New York, NY 10032, USA. [3]Department of Physiology and Cellular Biophysics, Columbia University Irving Medical Center, New York, NY 10032, USA. [4]Department of Pathology and Cell Biology, Columbia University Irving Medical Center, New York, NY 10032, USA.
*These authors contributed equally to this work.
†Present address: Department of Medicine, Division of Cardiovascular Medicine, Vanderbilt University Medical Center, Nashville, TN 37232, USA.
‡Present address: Vanderbilt Institute for Infection, Immunology and Inflammation, Vanderbilt University, Nashville, TN 37232, USA.
§Present address: Department of Molecular Physiology and Biophysics, Vanderbilt University, Nashville, TN 37232, USA.
‖Present address: Immunomic Therapeutics Inc., Rockville, MD 20850, USA.
¶Corresponding author. Email: ofarokhzad@bwh.harvard.edu (O.C.F.); iat1@columbia.edu (I.T.); jshi@bwh.harvard.edu (J.S.)

Downloaded from http://stm.sciencemag.org/ at Columbia University Libraries on July 30, 2020

cap thickness, and inhibits atherosclerotic plaque necrosis. This study demonstrates the use of siRNA-containing NPs to silence genes in lesional macrophages and shows the therapeutic potential of this strategy when applied to a specific macrophage molecule involved in advanced plaque progression.

RESULTS

Synthesis and characterization of S2P-conjugated siRNA NPs

The targeted siRNA NPs were designed on the basis of the following considerations (*17*, *19*–*23*): (i) increased blood circulation time to facilitate permeation through sites in the vasculature with leaky endothelium, which includes atherosclerotic lesions; (ii) nanoscale size and homing properties to enhance both plaque permeation and macrophage endocytosis; and (iii) effective late endosomal escape of the siRNA to enable gene silencing. These siRNA NPs were formulated by an optimized self-assembly method according to our previous reports (*14*, *15*). A cationic lipid–like material G0-C14 (*24*) was used to complex with siRNA, whereas a clinically used polymer, PLGA, formed a stable NP core to carry the G0-C14/siRNA complexes (Fig. 1A). Further, an S2P peptide (CRTLTVRKC) was conjugated to 1,2-distearoyl-*sn*-glycero-3-phosphoethanolamine-*N*-[maleimide(polyethylene glycol)] (DSPE-PEG-Mal) through maleimide chemistry to enhance macrophage targeting (fig. S1) (*16*–*18*). To optimize the surface chemistry and targeting efficacy of the siRNA NPs, different ratios of DSPE-PEG-S2P and DSPE-PEG were tested. Moreover, we considered the possibility that too high a content of S2P peptide might shield the PEG layer in a manner that would render the NPs unstable. In this context, 50% (w/w) of the DSPE-PEG-S2P in the lipid-PEG layer (denoted as $S2P_{50}$) appeared to be near the critical point (the maximum content of the targeting components) for maintaining NP stability (fig. S2). NPs with a DSPE-PEG-S2P ratio of 60% showed marked precipitation after 24 hours of incubation in phosphate-buffered saline (PBS) containing 10% serum, whereas NP formulations with an DSPE-PEG-S2P ratio ≤50% showed sufficient stability. Moreover, no obvious changes in NP size were observed over a period of 72 hours, further indicating the stability of our NPs (fig. S3). Because of the incorporation of targeting peptides on the surface, the engineered $S2P_{50}$ NPs showed a slightly increased diameter of 116.2 ± 2.5 nm versus 108 ± 2.8 nm for the nontargeted $S2P_0$ NPs as measured by dynamic light scattering (DLS), and a decreased zeta potential of −2.66 ± 1.01 mV versus −7.43 ± 0.94 mV for the $S2P_0$ NPs (Fig. 1, B and C). It should be noted that the siRNA encapsulation efficiency (EE) was similar between the $S2P_{50}$ and $S2P_0$ NPs (fig. S4). The spherical and uniform structure of the targeted $S2P_{50}$ NPs was revealed by transmission electron microscopy (TEM) imaging, and S2P has no obvious effect on NP morphology within the tested densities (fig. S5).

$S2P_{50}$ NPs protect siRNA from nuclease degradation and enable endosomal escape

To verify the ability of the engineered $S2P_{50}$ NPs to protect siRNA from serum nuclease degradation, we incubated the free siRNA or siRNA-encapsulated $S2P_{50}$ NPs in 100% murine serum at 37°C for different durations (0, 3, 6, 9, and 12 hours). The extracted siRNA from the $S2P_{50}$ NPs displayed no obvious degradation, whereas free siRNA was rapidly degraded in serum (fig. S6). These data show that the solid NP core can provide a stable and rigid nanostructure that protects the encapsulated siRNA.

To enable siRNA-mediated gene silencing, NP delivery platforms must allow the siRNA to escape from endosomes and be released into the cytoplasm (*25*, *26*). To assess escape of $S2P_{50}$ siRNA NPs from endosomes and their silencing efficacy, Dy647-labeled luciferase siRNA (siLuc) was incubated with luciferase-expressing HeLa (HeLa-Luc) cells. The internalized $S2P_{50}$-Dy647-siRNA NPs (red) were mainly colocalized with late endosomes (green) after the first 1 hour of incubation, whereas most of the NPs were located outside of endosomes after 4 hours of incubation, indicating release of the siRNA into the cytoplasm (Fig. 1D). We then tested silencing efficiency of these NPs by measuring luciferase expression in HeLa-Luc cells upon treatment. The HeLa-Luc cells in control groups showed high bioluminescence signals, whereas the treatment of $S2P_{50}$-siLuc NPs led to significantly reduced signals, with some areas even showing no bioluminescence ($P < 0.001$; Fig. 1E). In HeLa-Luc cells, the ability to silence luciferase was similar between $S2P_{50}$ siRNA NPs and $S2P_0$ siRNA (Fig. 1E and fig. S7, respectively). This was predicted, as the relative advantage conferred by S2P is relevant only to cells that express stabilin-2 and HeLa cells do not express stabilin-2. On the basis of analysis of cell viability, apoptosis, and proliferation assays, no obvious in vitro cytotoxicity was observed in different cell lines, including HeLa-Luc cells, RAW 264.7 macrophage cells, and human embryonic kidney (HEK) 293 cells, even at the highest siRNA concentration of 50 nM (figs. S8 to S10).

$S2P_{50}$ NPs target macrophages in atherosclerotic lesions

The targeting efficacy of the $S2P_{50}$ NPs was assessed both in cultured macrophages and in vivo. NPs of different densities of S2P were tested across multiple cell types, including T cells, dendritic cells (DCs), polymorphonuclear cells (PMNs), human umbilical vein endothelial cells (ECs), human aortic smooth muscle cells (SMCs), fibroblasts, cardiomyocytes, and macrophages. NP uptake in $CD4^+$ T cells, DCs, PMNs, and cardiomyocytes was low and could not be enhanced by increasing S2P ligand densities on the NP surface (fig. S11A), whereas NP uptake in ECs, SMCs, and fibroblasts was higher than in these other cells and was enhanced by increasing the density of S2P. Macrophages showed the most pronounced NP uptake (fig. S11, B and C). In addition, uptake of S2P-modified NPs by macrophages could be prevented by silencing stabilin-2 (fig. S11, B and C). These results indicate that macrophages show the most robust stabilin-2–dependent uptake of S2P-modified NPs, consistent with the fact that of the cell types assayed, macrophages have the highest stabilin-2 expression (fig. S11D). Because the $S2P_{50}$ NPs showed the highest uptake efficiency (Fig. 2A and fig. S11), we used this S2P-NP formulation in our subsequent studies.

To test the applicability of our NP platform in vivo, we first examined the pharmacokinetics of free Dy647-labeled siRNA, $S2P_0$-Dy647-siRNA NPs, and $S2P_{50}$-Dy647-siRNA NPs after intravenous injection into BALB/c mice. The circulating lifetime of siRNA was prolonged by both NP platforms ($t_{1/2} \approx 1.2$ hours for $S2P_{50}$ NPs; $t_{1/2} \approx 1.5$ hours for $S2P_0$ NPs) compared with free siRNA (rapidly cleared within 30 min) (fig. S12), which could improve the localization and plaque accumulation of the siRNA NPs (*19*). In addition, the targeting peptides had no obvious influence on the blood circulation of NPs, as evidenced by the similar circulation profile of the $S2P_{50}$-Dy647-siRNA NPs versus $S2P_0$-Dy647-siRNA NPs. We then tested the in vivo targeting capability of the NP platform in atherosclerotic lesions in $Ldlr^{-/-}$ mice that were fed a Western diet (WD) for 12 weeks. Alexa 647–labeled $S2P_{50}$ NPs or $S2P_0$ NPs loaded with

Downloaded from http://stm.sciencemag.org/ at Columbia University Libraries on July 30, 2020

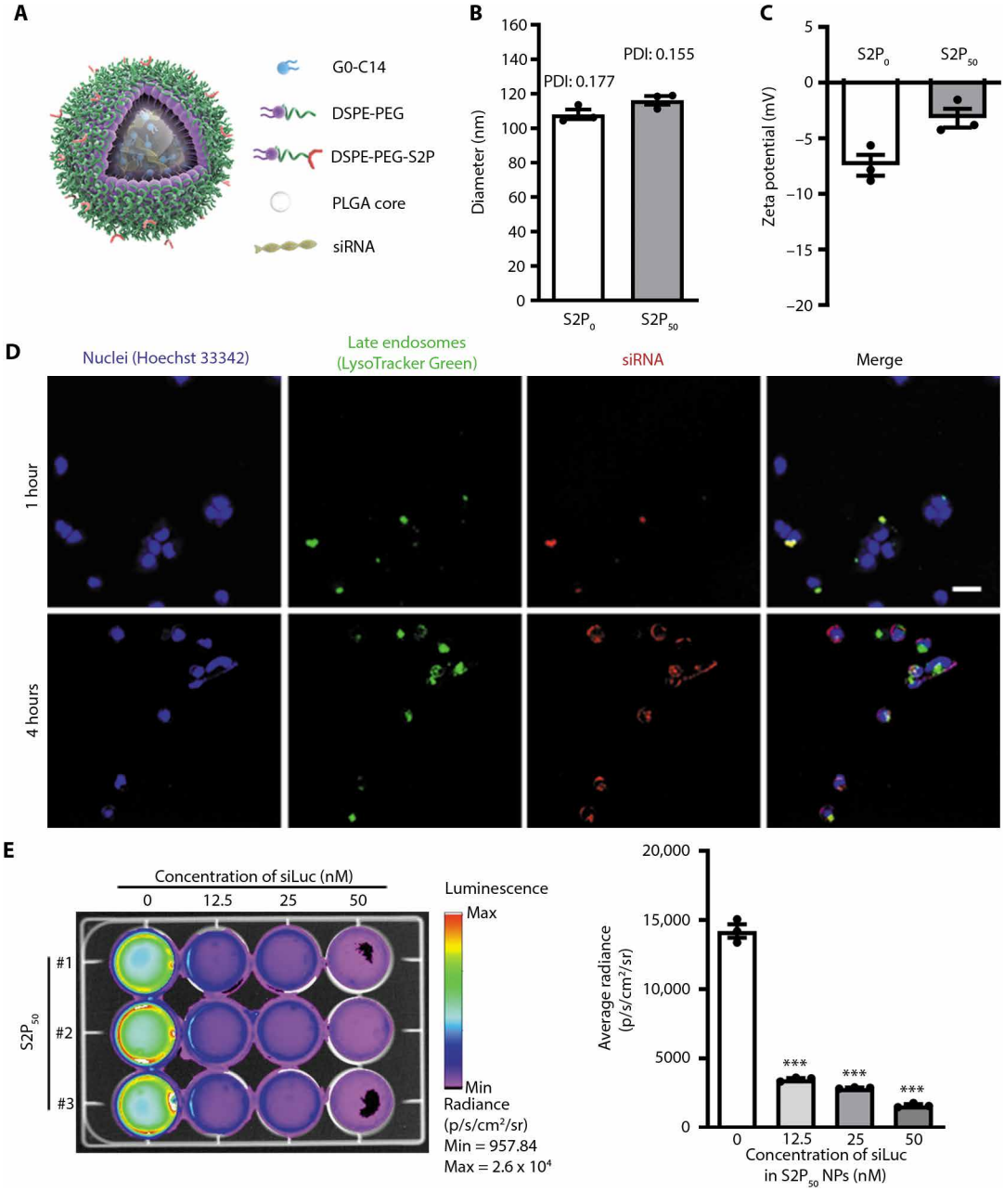

Fig. 1. Characterization, endosomal escape, and silencing efficacy of S2P-conjugated siRNA NPs. (**A**) Schematic diagram of targeted NP design. (**B** and **C**) NP diameter as assessed by DLS and zeta potential of nontargeted NPs ($S2P_0$) and targeted S2P-NPs ($S2P_{50}$) ($n = 3$ preparations of each type of NP, mean ± SEM). PDI, polydispersity index. (**D**) Laser scanning confocal microscopic images of HeLa-Luc cells after incubation for 1 or 4 hours with Dy647-siRNA (red)–loaded $S2P_{50}$ NPs. Nuclei were stained with Hoechst 33342 (blue), and late endosomes were stained with LysoTracker Green (green). Scale bar, 50 μm. (**E**) Bioluminescence imaging of luciferase-expressing HeLa (HeLa-Luc) cells after 24 hours of treatment with $S2P_{50}$ NPs loaded with the indicated concentrations of siLuc. The graph shows the average radiance of the cells ($n = 3$ plates of cell per group, mean ± SEM). Statistical significance was determined using one-way ANOVA (***$P < 0.001$).

siRNA (siCamk2g) were intravenously injected into these mice. Twenty-four hours after the injections, the aorta, kidneys, lungs, spleen, and liver were harvested. The fluorescent signals of Alexa 647 in the aorta were about twofold greater for the targeted $S2P_{50}$-siCamk2g NPs than for the nontargeted $S2P_0$-siCamk2g NPs (Fig. 2B). Flow cytometry analysis of disaggregated aortas revealed that Alexa 647–labeled $S2P_{50}$ NPs were specifically taken up by $CD45^+F4/80^+$ macrophages compared with nonimmune $CD45^-$ cells in atherosclerotic lesions (Fig. 2C and fig. S13). Moreover, the S2P modification enhanced macrophage uptake of NPs by almost threefold compared with non–S2P-modified NPs. As the first-pass effect occurs in the liver, and as the spleen contains a large population of macrophages, it is expected that NPs also accumulated in these two organs, with a higher amount of $S2P_{50}$-siCamk2g versus $S2P_0$-siCamk2g NPs in the spleen (fig. S14).

Downloaded from http://stm.sciencemag.org/ at Columbia University Libraries on July 30, 2020

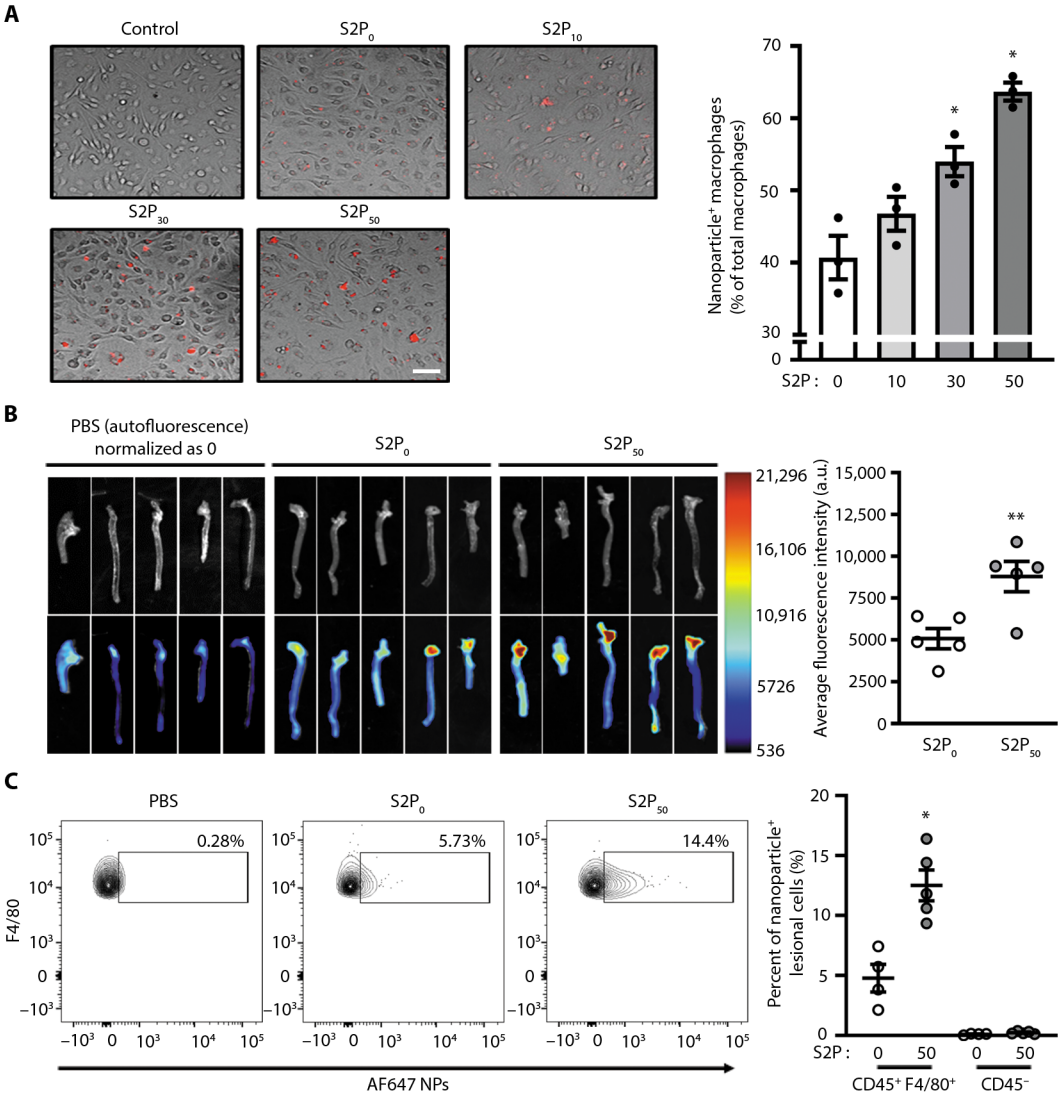

Fig. 2. Uptake of siRNA-loaded NPs by macrophages and localization in aorta after injection into WD-fed *Ldlr*$^{-/-}$ mice. (**A**) Bone marrow–derived macrophages (BMDMs) were incubated for 2 hours without (control) or with Dy647-labeled NPs with the indicated percentage of S2P modifications and with an siRNA concentration of 50 nM. After the cells were rinsed and fixed, fluorescence images were captured. Representative merged bright-field fluorescence images are shown. The percent uptake of labeled NPs was quantified by counting ($n = 3$ plates of BMDMs per group, mean ± SEM). Statistical significance was determined using one-way ANOVA (*$P < 0.05$ versus 0 and 25 S2P groups). Scale bar, 25 μm. (**B**) Twelve-week WD-fed *Ldlr*$^{-/-}$ were injected intravenously with nontargeted Alexa 647–conjugated $S2P_0$-siCamk2g NPs or Alexa 647–conjugated $S2P_{50}$-siCamk2g NPs at a dose of 1 nmol of siRNA per mouse. The mice received another injection 24 hours later. Twenty-four hours after the second injection, the mice were euthanized, and the aortas were imaged and quantified using ImageJ software ($n = 5$, mean ± SEM). Statistical significance was determined using Student's *t* test. **$P < 0.01$. (**C**) Representative flow plots and quantification of macrophages containing AF647-labeled NPs in aortas harvested from 8-week WD-fed *Ldlr*$^{-/-}$ mice 24 hours after they were injected intravenously with PBS, $S2P_0$ AF647-NPs, or $S2P_{50}$ AF647-NPs. Aortic cells were isolated and then immunostained for CD45 and F4/80 followed by flow cytometry analysis ($n = 4$ to 5 mice per group, mean ± SEM). Statistical significance was determined using Student's *t* test. *$P < 0.05$. a.u., arbitrary unit.

Similar to lesional macrophages, splenic macrophages also showed enhanced NP uptake with the S2P modification (fig. S15).

$S2P_{50}$-siCamk2g NPs silence CaMKIIγ in lesional macrophages and promote plaque stabilization

To test the silencing efficiency of $S2P_{50}$-siCamk2g NPs in macrophages, we treated bone marrow–derived macrophages (BMDMs) with control siRNA (CtrRNA)–loaded $S2P_{50}$ NPs or siCamk2g-loaded $S2P_{50}$ NPs and analyzed the protein expression of CaMKIIγ. The data show that CaMKIIγ was decreased by ~60% (Fig. 3A). As deletion of CaMKIIγ increases the expression of MerTK in macrophages (*12*), we also assessed MerTK expression and found that it was increased in $S2P_{50}$-siCamk2g NP–treated macrophages (Fig. 3A). Moreover, macrophages treated with $S2P_{50}$-siCamk2g NPs showed increased efferocytosis (figs. S16 and S17). To test the ability of $S2P_{50}$-siCamk2g NPs to silence CaMKIIγ in atherosclerotic lesional macrophages, *Ldlr*$^{-/-}$ mice were fed a high-fat WD for 8 weeks and then injected intravenously twice a week for 4 weeks with PBS, $S2P_{50}$ NPs carrying 1 nmol of CtrRNA, or $S2P_{50}$ NPs carrying 1 nmol of siCamk2g. Immunostaining of lesions for CaMKIIγ and

Downloaded from http://stm.sciencemag.org/ at Columbia University Libraries on July 30, 2020

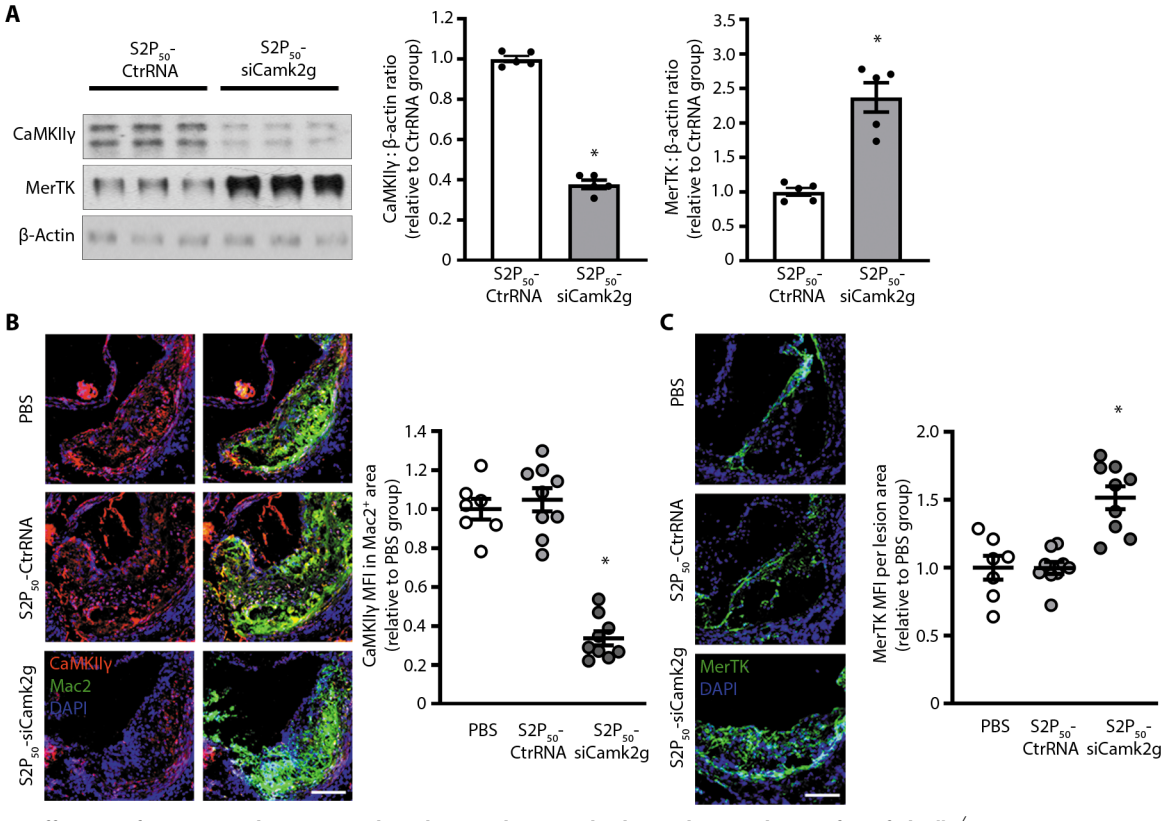

Fig. 3. Silencing efficiency of S2P$_{50}$-siCamk2g NPs in cultured macrophages and in lesional macrophages of WD-fed *Ldlr*$^{-/-}$ mice. (**A**) BMDMs were treated with S2P$_{50}$ NPs delivering either 50 nM control siRNA (CtrRNA) or 50 nM siCamk2g. Three days after NP treatment, the cells were lysed and immunoblotted for MerTK, CaMKIIγ, and β-actin. Immunoblots and quantified densitometric data are shown ($n = 5$ plates of macrophages per group). Data were nonparametric, and statistical significance was determined using a Mann-Whitney *U* test. *$P < 0.05$. (**B** and **C**) Eight-week WD-fed *Ldlr*$^{-/-}$ were injected intravenously twice a week with PBS, S2P$_{50}$ NPs loaded with CtrRNA (1 nmol of CtrRNA per injection), or S2P$_{50}$ NPs carrying siCamk2g (1 nmol of siCamk2g per injection) for another 4 weeks while being maintained on the WD. Cross sections of the aortic root were immunostained for CaMKIIγ, MerTK, and Mac2 and counterstained with DAPI. Scale bars, 200 μm. The staining data were quantified using FIJI software as mean fluorescence intensity (MFI) relative to the PBS group as follows: using Mac2$^+$ area for CaMKIIγ and total lesion area for MerTK as the denominators ($n = 7$ to 9 mice per group). Data were normal, and statistical significance was determined using one-way ANOVA. *$P < 0.05$ versus the other two groups.

macrophages showed marked decrease in the enzyme in lesional macrophages in the S2P$_{50}$-siCamk2g NP cohort versus the other two cohorts (Fig. 3B). We also examined CaMKIIγ silencing efficiency in other cell types in the plaques, including SMCs and ECs. Consistent with the fact that S2P-modified NPs are not taken up by CD45$^-$ cells in atherosclerotic plaques, there was minimal CaMKIIγ silencing in ECs and SMCs (fig. S18). We also observed silencing of CaMKIIγ in both splenic and liver macrophages (figs. S19 and S20, respectively), which is consistent with the biodistribution data showing NPs in the spleen and liver.

Further, as predicted from our previous study and the above data, macrophage MerTK staining was increased in the lesions of the S2P$_{50}$ NP–treated mice (Fig. 3C). Thus, treatment of atherosclerotic mice with S2P$_{50}$-siCamk2g NPs successfully lowers lesional macrophage CaMKIIγ and induces a biological process downstream of CaMKIIγ, namely, an increase in MerTK.

S2P$_{50}$-siCamk2g NPs improve efferocytosis, increase fibrous cap thickness, and decrease necrotic core areas in WD-fed *Ldlr*$^{-/-}$ mice

To determine the therapeutic potential of S2P$_{50}$-siCamk2g NPs, we designed a study that specifically tested whether silencing CaMKIIγ in established plaques would reduce features associated with plaque instability. *Ldlr*$^{-/-}$ mice were fed the WD for 8 weeks and then intravenously injected with PBS, S2P$_{50}$-CtrRNA NPs, or S2P$_{50}$-siCamk2g NPs twice a week for an additional 4 weeks while the mice were maintained on the WD. The lesions of the S2P$_{50}$-siCamk2g NP cohort showed reduced necrotic core area and reduced ratio of necrotic core area to lesion size, whereas collagen cap thickness was enhanced, indicating increased plaque stability (Fig. 4, A to E). Because lesional MerTK expression is enhanced in mice treated with S2P$_{50}$-siCamk2g NPs, we next tested whether lesional macrophages had an increased ability to execute efferocytosis. Aortic root cross sections were assayed by immunofluorescence microscopy for TUNEL$^+$ (terminal deoxynucleotidyl transferase–mediated deoxyuridine triphosphate nick end labeling–positive) apoptotic cells (ACs) that were either associated with Mac2$^+$ macrophages, which indicates efferocytosis, or "free" of macrophages. The ratio of macrophage-associated ACs to free ACs was significantly increased in the lesions of mice treated with S2P$_{50}$-siCamk2g NPs ($P < 0.05$; Fig. 4F), indicative of enhanced efferocytosis. Relevant systemic features, including total cholesterol, blood glucose, body weight, and blood leukocytes, neutrophils, lymphocytes, monocytes, eosinophils, basophils, Ly6C^{high}, and Ly6C^{low} cells, and circulating tumor

Downloaded from http://stm.sciencemag.org/ at Columbia University Libraries on July 30, 2020

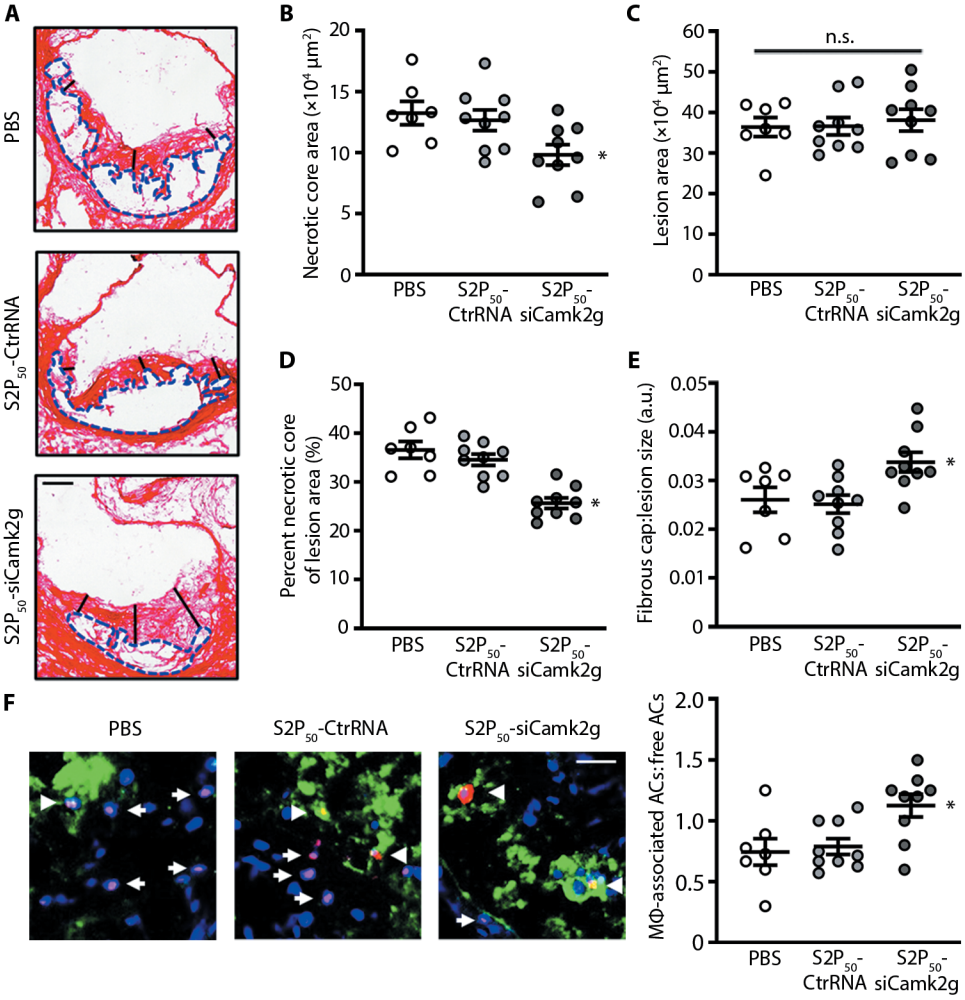

Fig. 4. Treatment of WD-fed Ldlr$^{-/-}$ mice with S2P$_{50}$-siCamk2g–loaded NPs lowers plaque necrosis and increases lesional efferocytosis. (**A** to **F**) Aortic roots from the mice in Fig. 3 (B and C) were stained with picrosirius red and quantified for lesion size and necrotic core area. The collagen cap thickness was measured at the midpoint and shoulder regions of each lesion and quantified as the ratio of cap thickness to lesion size. Lesional efferocytosis was quantified as the ratio of TUNEL$^+$ cells (red) associated with Mac2$^+$ macrophages (green) to free TUNEL$^+$ cells. Arrows represent free TUNEL$^+$ cells, and arrowheads represent TUNEL$^+$ cells associated with Mac2$^+$ macrophages. Scale bars, 200 μm (A) and 50 μm (F). For all data, $n = 7$ to 9 mice per group. Statistical significance was determined using one-way ANOVA. *$P < 0.05$ versus the other two groups; n.s., not significant.

necrosis factor–α (TNF-α) were similar among the three groups of mice (fig. S21). These data demonstrated that targeted siRNA NPs can be used to silence a plaque-destabilizing gene in lesional macrophages and thereby stabilize plaques.

In vivo toxicity of S2P$_{50}$-siCamk2g NPs

To test the in vivo toxicity of the targeted S2P$_{50}$-siCamk2g NPs, hematological, blood biochemical, and histological end points were investigated in healthy BALB/c mice after different treatment regimens. For acute toxicity studies, S2P$_{50}$-siCamk2g NPs were injected intravenously once daily for five continuous days, and for long-term toxicity studies, S2P$_{50}$-siCamk2g NPs were injected intravenously twice per week for 4 weeks. Mice treated with PBS were used as controls. Three days after the last injection, the acutely and chronically treated mice were euthanized, and hearts, livers, spleens, lungs, kidneys, and blood were harvested. Analysis of hematoxylin and eosin (H&E)–stained organs revealed no obvious signs of organ injury (Fig. 5, A and B), which was also confirmed in the above *Ldlr*$^{-/-}$ mouse model receiving 4 weeks of NP treatment (two injections per week; fig. S22). There were also no significant differences in hematological parameters, including red blood cell count (RBC), white blood cell count (WBC), neutrophil count (NPC), mean corpuscular volume (MCV), mean corpuscular hemoglobin concentration (MCHC), lymphocyte count (LY), hematocrit (HCT), and hemoglobin (Hb), or in alanine aminotransferase (ALT), aspartate aminotransferase (AST), and blood urea nitrogen (BUN) (Fig. 5, C and D). Last, in a separate experiment, we assayed plasma for TNF-α and interleukin-12 (IL-12) 24 hours after a single intravenous injection of PBS, empty S2P$_{50}$ NPs, or S2P$_{50}$-siCamk2g NPs and found no difference among the three groups of mice (fig. S23). These combined data indicate that the NP platform used in this study is not overtly toxic when administered to mice over the short term or long term.

DISCUSSION

The overall objective of this study was to determine whether a targeted siRNA NP platform could be used to silence the expression of a plaque-destabilizing gene in atherosclerotic lesional macrophages and thereby promote plaque stability. As a test case, we chose macrophage *Camk2g* as the gene target, because we have shown previously that conventional gene targeting of this gene in myeloid cells, such as using *Lyz2Cre Camk2g*$^{fl/fl}$ mice, in an atherosclerosis mouse model promotes plaque stability by a well-defined mechanism (*12*). In that report, data with human macrophages and human atheroma provided evidence that activation of CaMKIIγ in lesional macrophages promotes advanced plaque progression in humans (*12*). The data reported here show that S2P$_{50}$-siCamk2g NPs successfully silence CaMKIIγ in macrophages both in vitro and in atherosclerotic lesions. Moreover, consistent with our previous mechanistic studies, treatment of atherosclerotic mice with these NPs promotes plaque stability, including increased expression of the efferocytosis receptor MerTK in lesional macrophages and increased efferocytosis (fig. S24). Thus, in addition to establishing the concept that targeted siRNA NPs can be used for gene silencing in atherosclerotic lesional macrophages, the example used herein can now be considered as a type of new strategy to combat acute atherothrombotic vascular disease. This disease, manifested as myocardial infarction, unstable angina, sudden coronary death, and stroke, is a

Downloaded from http://stm.sciencemag.org/ at Columbia University Libraries on July 30, 2020

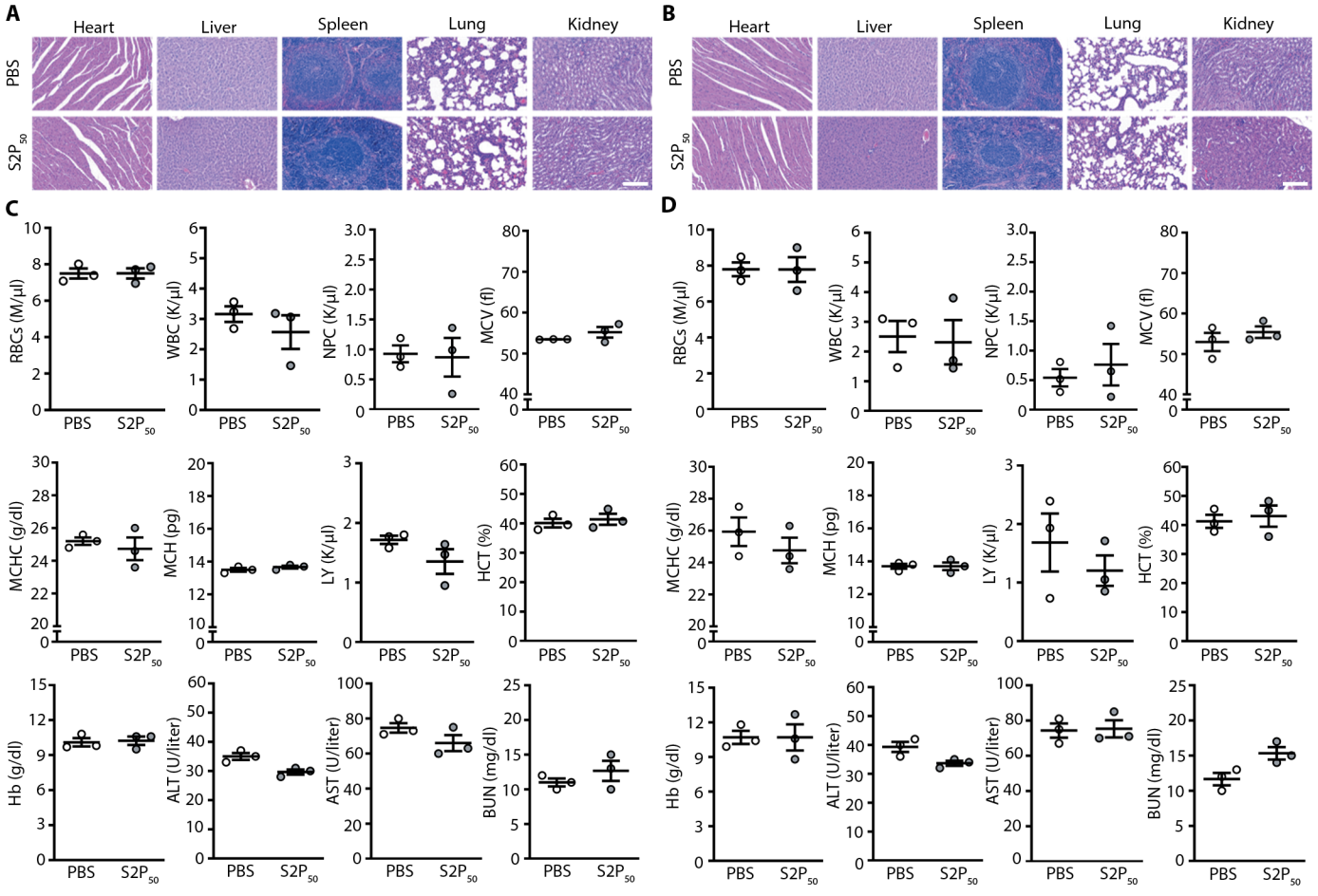

Fig. 5. In vivo safety evaluation of the targeted $S2P_{50}$-siCamk2g NPs by hematological, blood biochemical, and histological analyses. Female BALB/c mice were injected intravenously with either PBS or $S2P_{50}$-siCamk2g NPs at a dose of 1 nmol siRNA per mouse. For acute toxicity studies (**A** and **C**), treatment with PBS or $S2P_{50}$-siCamk2g NPs was carried out for five consecutive days, with one injection per day. For long-term toxicity studies (**B** and **D**), treatment with PBS or $S2P_{50}$-siCamk2g NPs was carried out for 4 weeks, with two injections per week. Three days after the last injection, the mice were euthanized and the indicated organs were sectioned and stained with H&E. Scale bars, 100 μm. Blood was analyzed for the indicated biochemical and hematological end points ($n = 3$ mice per group, mean ± SEM). The tested parameters include red blood cell count (RBC), white blood cell count (WBC), neutrophil count (NPC), mean corpuscular volume (MCV), mean corpuscular hemoglobin concentration (MCHC), lymphocyte count (LY), hematocrit (HCT), hemoglobin (Hb), alanine aminotransferase (ALT), aspartate aminotransferase (AST), and blood urea nitrogen (BUN). None of the differences between PBS and $S2P_{50}$ groups were statistically significant as determined by Student's *t* test.

major cause of death throughout the world, and it is the minority of lesions that become unstable that is a key root cause of these clinical events (*13*). Thus, specifically targeting a cellular mechanism of vulnerable plaque formation would be expected to have great promise in preventing acute vascular disease.

RNAi technology can target any gene of interest and has been widely used to identify and validate putative therapeutic targets (*3*, *27*). RNAi can also robustly modulate genes and pathways that are considered "undruggable" or need time-consuming and complex development of effective inhibitors (*2*, *28*). With recent FDA approval of the first siRNA product for the treatment of a disease, hereditary transthyretin amyloidosis (*6*), we anticipate that RNAi-based therapies will be validated as a treatment strategy for other diseases. Different NP platforms have been developed for delivery of conventional drugs (such as pitavastatin, simvastatin, liver X receptors agonist, pioglitazone, and TRAF6 inhibitor) to macrophages (*21*, *29*–*35*), and targeted macrophage ablation could also be achieved via light-activated NP platforms (*36*, *37*). Another study demonstrated that NP-mediated siRNA delivery targeting CCR2 to a subset of circulating monocytes can reduce atherosclerosis (*38*). However, to our best knowledge, NP-based specific delivery of siRNA to atherosclerotic lesional macrophages has not previously been reported.

To address the barriers associated with systemic siRNA delivery, including rapid clearance, nuclease degradation, poor plaque targeting and accumulation, lack of specific and effective uptake by macrophages, and insufficient endosomal release of the siRNA to the cytoplasm, we designed a unique lipid-polymer NP platform. Cationic G0-C14 was developed to effectively absorb the siRNA and enable its escape from late endosomes (*39*, *40*), whereas clinically approved PLGA polymer was used to encapsulate the siRNA/C0-C14 complexes, protect the siRNA from serum nuclease degradation, and enable good biocompatibility (*14*, *24*). The lipid-PEG (DSPE-PEG) was used to stabilize the NPs, achieve an increased circulating lifetime,

Downloaded from http://stm.sciencemag.org/ at Columbia University Libraries on July 30, 2020

and avoid rapid clearance (*41*, *42*). A plaque macrophage–targeting peptide (S2P), which binds to the macrophage stabilin-2 receptor (*16*–*18*), was incorporated on the lipid-PEG layer of the NP surface. Our results demonstrate that siCamk2g can be efficiently encapsulated in ~100-nm targeted NPs, which are within the preferred size range for effective enhanced permeability and retention, which is a key feature that promotes NP entry into the arterial wall at sites where the endothelial barrier is impaired (*43*). In the context of our previous studies using targeted polymeric NPs to deliver biologics, e.g., proteins and peptides, to atherosclerotic plaques (*19*, *20*, *44*), this study extends to the application of siRNA NPs to target specific signaling pathways in a specific cell type in the plaque tissue.

In summary, as proof of concept of using a targeted siRNA NP platform to silence gene expression in atherosclerotic lesional macrophages, we show that treatment of mice with established atherosclerosis with $S2P_{50}$-siCamk2g NPs reduces CaMKIIγ expression in lesional macrophages and promotes plaque stabilization. As the current study is limited to the WD-fed *Ldlr*$^{-/-}$ mouse model, additional confirmatory studies will be needed to further validate this strategy for potential translation, including evaluation in larger preclinical models such as fat-fed pigs and nonhuman primates. As continuous long-term treatment is generally required for chronic diseases such as atherosclerosis, the siRNA NPs can be further optimized to reduce the dosing frequency and prolong the silencing effect, for example, by using fully chemically modified siRNA with drastically enhanced stability. In addition, more robust formulation strategies may be required for the scale-up and manufacturing of such targeted siRNA NPs. Considering the key role of macrophages in atherosclerosis (*1*, *45*), this strategy can be applied for silencing other genes in lesional macrophages shown to be important in human atherosclerosis, such as those involved in inflammasome activation of IL-1β secretion (*46*). It remains elusive whether concurrent delivery of multiple siRNAs against different pro-atherogenic macrophage pathways may lead to synergistic efficacy. Moreover, the findings herein may shed light on the application of NP-mediated delivery of other types of RNA therapeutics, such as microRNA and mRNA, to lesional macrophages for the purpose of exploring and validating new targets and pathways in the treatment of atherosclerosis.

MATERIALS AND METHODS

Study design

The aim of this study was to rationally develop targeted siRNA NPs that can specifically silence a plaque-destabilizing molecule—CaMKIIγ in atherosclerotic lesional macrophages, and to verify the therapeutic efficacy of this strategy in atherosclerotic mice. The physicochemical properties of the targeted siCamk2g NPs were characterized by measuring size, morphology, zeta potential, EE, and stability. Capabilities of the targeted NPs in endosomal escape, lesional macrophage targeting, and gene silencing were verified through different experiments. Animal studies were performed in WD-fed Ldlr$^{-/-}$ mice (for evaluating the targeting ability and therapeutic efficacy in vivo, and for mechanistically clarifying the therapeutic principles) and BALB/c mice (for confirming the in vivo safety of the targeted siRNA NPs) according to the protocols approved by the Institutional Animal Care and Use Committees at Columbia University and Brigham and Women's Hospital, respectively. Mice were randomly assigned to each study group. All experiments in this study were conducted with at least three independent replicates (specified in the figure legends). The researchers were not blinded to the identity of the study groups.

Synthesis of lipids and polymers

The S2P peptide–conjugated lipid-PEG was synthesized by conjugating CRTLTVRKC peptide (GLS Biochem Systems Inc., catalog no. 652358) to DSPE-PEG-Mal [PEG molecular weight (MW), 3.4 kDa; Nanocs Inc., catalog no. PG2-DSML-3k) via the free thiol of the C terminus using maleimide chemistry. The final products were washed and purified in cold methanol and characterized by ^{1}H nuclear magnetic resonance (NMR). The cationic G0-C14 was synthesized from 1,2-epoxytetradecane (Sigma-Aldrich, catalog no. 260266) and PAMAM dendrimer G0 (Sigma-Aldrich, catalog no. 412368) at a molar ratio of 7:1 by a ring-opening reaction according to our previous reports (*14*, *24*). The fluorescent PLGA–Alexa 647 polymer was synthesized by coupling Alexa Fluor 647 Cadaverine (Thermo Fisher Scientific, catalog no. A30679) to the C terminus of 50:50 PLGA (inherent viscosity range of 0.55 to 0.75 dl/g, 43.4 kDa, LACTEL Absorbable Polymers by DURECT Corporation, catalog no. B6013-2).

Formulation of siRNA-loaded NPs

The targeted NPs were prepared by a modified, robust self-assembly method based on our previous studies (*14*, *15*). Briefly, 2 nmol of siRNA in 20 μl of nuclease-free HyPure water (GE Healthcare Life Sciences, catalog no. SH30538) was mixed with 250 μg of G0-C14 in 100 μl of acetone (2.5 mg/ml) for 10 s to form siRNA/G0-C14 complexes and enable full electronic interactions. Then, PLGA (2.5 mg in 500 μl of acetone) was further added followed by gentle mixing to achieve a homogeneous solution. The solution was subsequently added dropwise to 10 ml of HyPure water containing 1 mg of hybrid lipid-PEGs, i.e., DSPE-PEG-S2P/DSPE-PEG hybrids at different ratios. The targeted NPs formed instantly upon mixing. After magnetic stirring at 1000 rpm for 1 hour, the NPs were collected by centrifugation for 20 min at 4000 rpm using Amicon Ultra-15 centrifugal filter units [MW cutoff (MWCO), 100 kDa; Millipore, catalog no. UFC9100], followed by washing three times with HyPure water. Last, the NPs were resuspended in PBS (GE Healthcare Life Sciences, catalog no. SH30256) at different concentrations. Using this procedure, we made targeted NPs with four different DSPE-PEG-S2P/DSPE-PEG ratios (w/w): $S2P_{10}$, 10% of DSPE-PEG-S2P in lipid-PEG layer; $S2P_{30}$, 30% of DSPE-PEG-S2P in lipid-PEG layer; $S2P_{50}$, 50% of DSPE-PEG-S2P in lipid-PEG layer; and $S2P_{60}$, 60% of DSPE-PEG-S2P in lipid-PEG layer. For nontargeted NP preparation, all the steps were the same, except that only nontargeted DSPE-PEG (MW, 3 kDa; Avanti Polar Lipids, catalog no. 880320) was used to construct the lipid-PEG layer of the NPs (named $S2P_0$ NPs). For the fluorescent NP preparation, PLGA/PLGA–Alexa 647 hybrid polymers at the weight ratio of 1:1 were used instead of pure PLGA to construct the solid polymeric core.

Physicochemical characterization and stability of siRNA-loaded NPs

The targeted and nontargeted siRNA NPs were characterized by size, zeta potential, EE, morphology, and stability. The size and zeta potential were measured by DLS (Brookhaven Instruments Corporation). The morphology and shape of the NPs were assessed by a transmission electron microscope using a JEOL 1200EX electron

Downloaded from http://stm.sciencemag.org/ at Columbia University Libraries on July 30, 2020

microscope at 80 kV. The EE is defined by the fraction of added siRNA that is encapsulated by the NPs. To measure the siRNA EE, NPs loaded with Dy647-labeled siRNA (Dy647-siRNA) were made according to the method described above. A 5-μl volume of the NP solution was mixed with 95 μl of dimethyl sulfoxide, and the fluorescence intensity of the extracted Dy647-siRNA was determined by an Infinite M200 PRO spectrophotometer (TECAN) and compared to a 1 nmol/ml solution of free Dy647-siRNA. EE is defined as the fraction of fluorescent siRNA added during the NP construction procedure that was extracted from the purified NPs. To check the in vitro stability of the NPs, they were incubated with PBS containing 10% serum and then subjected to 24 hours of rotation at 37°C at 100 rpm, after which the degree of dispersion was observed and recorded by a camera. To evaluate the protection of siRNA by the NPs, free siRNAs or siRNA-loaded $S2P_{50}$ NPs were added to 100% serum at a volume ratio of 1:1 and then incubated at 37°C for 3, 6, 9, or 12 hours. The NPs were then collected by centrifugation at 4000 rpm for 15 min using Amicon Ultra-15 centrifugal filter units (MWCO, 100 kDa). Chloroform was used to dissolve the pellet, and the siRNA was extracted in 0.5 M NaCl containing 0.1% SDS (*14*). The free siRNA and NP-extracted siRNA were subjected to electrophoresis on ethidium bromide–infused E-Gel 4% agarose gels (Thermo Fisher Scientific, catalog no. G501804) and imaged under ultraviolet (UV) light.

Assessment of endosomal escape of NP-siRNA

HeLa-Luc cells were seeded in Nunc glass bottom dishes (Thermo Fisher Scientific, catalog no. 150680) at a density of 2×10^5 cells per well and incubated for 24 hours in 1 ml of RPMI 1640 medium containing 10% fetal bovine serum (FBS). Dy647-siRNA–loaded $S2P_{50}$ NPs were then added and incubated with the cells for 1 or 4 hours. The medium was then removed, and the cells were rinsed three times with PBS. Hoechst 33342 (Thermo Fisher Scientific, catalog no. H1399) was used to stain the nuclei, and LysoTracker Green (Thermo Fisher Scientific, catalog no. L7526) was used to stain late endosomes. The cells were observed and imaged using an FV1000 laser scanning confocal microscope (Olympus).

In vitro assessment of gene silencing by siRNA-loaded NPs

HeLa-Luc cells were seeded in 12-well plates at the density of 10^6 cells per well and incubated for 24 hours in 1 ml of RPMI 1640 medium containing 10% FBS. The cells were then incubated with siLuc-loaded NPs for 24 hours, followed by washing with fresh medium and a 5-min incubation with Steady-Glo Luciferase Assay System (Promega Corporation, catalog no. E2520). Firefly luciferase expression was assessed by quantifying bioluminescence using an In-Vivo Xtreme imaging system with a charge-coupled device (CCD) camera. Bruker MI SE software was used to quantify the average radiance (photons per second per cm^2 per steradian) within regions of interest, and GraphPad software was used to plot the changes of average radiance.

In vitro toxicity study

HeLa-Luc, RAW 264.7, and HEK-293 cells were cultured in 96-well plates at the density of 5000 cells per well and allowed to adhere overnight. The cells were then transfected with siLuc-loaded $S2P_{50}$ NPs at the indicated concentrations. After 24 hours, the medium was removed and replaced with fresh medium, and after an additional 48 hours, cytotoxicity was assayed using the alamarBlue cell viability reagent (Thermo Fisher Scientific, catalog no. DAL1025) according to the manufacturer's protocol.

Animals

Six- to eight-week-old male C57BL/6J mice, 6-week-old female and male BALB/c mice, and 8- to 10-week-old male $Ldlr^{-/-}$ mice were purchased from the Jackson laboratory (Bar Harbor, ME). All procedures were conducted in accordance with protocols approved by the Institutional Animal Care and Use Committees at Harvard Medical School and Columbia University Irving Medical Center.

BMDMs and Jurkat cells

C57BL/6J mice were euthanized with isoflurane, and hind legs were removed. Femurs and tibias were flushed using a 26-gauge needle with Dulbecco's modified eagle medium (DMEM) containing glucose (4.5 g/liter), 20% L929 cell-conditioned media, 10% heat-inactivated FBS, penicillin (10 U/ml), and streptomycin (100 μg/ml). Cell suspensions were passed over a 40-μm filter, centrifuged at 500*g*, resuspended in 50 ml of media, and plated into five 100-mm dishes. Cells were incubated for 4 days, after which nonadherent cells and debris were aspirated, and the medium was replaced with fresh medium. After 7 to 10 days of differentiation, with media changed every 2 to 3 days, the cells were harvested for use in the indicated experiments. Jurkat cells were cultured in DMEM containing glucose (4.5 g/l), 10% (v/v) heat-inactivated FBS, penicillin (10 U/ml), and streptomycin (100 μg/ml).

Macrophage uptake of Dy647-labeled NPs

BMDMs were incubated for 2 hours with Dy647-labeled NPs with varying S2P modifications at an siRNA concentration of 50 nM. Cells were rinsed twice with 1× PBS and then fixed in 4% formaldehyde for 20 min. Fluorescence images were captured with an Olympus DP71 CCD camera attached to an Olympus IX-70 inverted epifluorescence microscope.

In vitro efferocytosis

BMDMs were plated at 0.15×10^6 cells per well in 24-well plates and allowed to adhere overnight and then incubated with $S2P_{50}$ NPs carrying either control siRNA or siCamk2g siRNA at a concentration of 50 nM siRNA. After 3 days, Jurkat cells were labeled with PKH67 per the manufacturer's directions, resuspended in DMEM with 10% heat-inactivated (HI)–FBS, and exposed to UV light (254 nm, Analytik Jena US LLC) for 15 min to induce apoptosis. After two additional hours of culture, ~85% of the Jurkat cells were apoptotic. These ACs were added to the BMDMs at a cell ratio of 3:1 (ACs:macrophages). After 45 min of incubation, the medium was removed, and the BMDMs were rinsed twice with PBS. The BMDMs were then fixed with 4% formaldehyde for 20 min, and images were captured with an Olympus DP71 CCD camera attached to an Olympus IX-70 inverted epifluorescence microscope. The percentage of BMDMs with engulfed PKH67-labeled ACs was quantified.

Pharmacokinetics study

BALB/c mice were randomly divided into three groups and injected intravenously with free Dy647-siRNA, nontargeted Dy647-siRNA–loaded $S2P_0$ NPs, or targeted Dy647-siRNA–loaded $S2P_{50}$ NPs at the siRNA dose of 1 nmol per mouse. After the indicated times, 20 μl of orbital vein blood was withdrawn from each mouse using a pipette tip containing heparin. The wound was then pressed for 30 s

Downloaded from http://stm.sciencemag.org/ at Columbia University Libraries on July 30, 2020

with an alcohol pad to stop the bleeding. The fluorescence intensity of the Dy647-siRNA in the blood was determined by an Infinite M200 PRO spectrophotometer (TECAN).

Biodistribution of siCamk2g NPs in WD-fed *Ldlr*$^{-/-}$ mice

Male *Ldlr*$^{-/-}$ mice fed a WD (TD.88137, 21.2% fat by weight, 48.5% carbohydrate by weight, and 17.3% protein by weight; Envigo) for 12 weeks were injected intravenously with nontargeted Alexa 647–conjugated S2P$_0$-siCamk2g NPs or Alexa 647–conjugated S2P$_{50}$-siCamk2g NPs at a dose of 1 nmol of siRNA per mouse. The mice received another injection 24 hours later. Twenty-four hours after the second injection, the mice were euthanized, and the aorta, kidneys, lungs, spleen, and liver were harvested and imaged using a CRi Maestro II In-Vivo Imaging System (Cambridge Research & Instrumentation Inc.). The imaging data were quantified using ImageJ.

In vivo toxicity evaluation

Female BALB/c mice were injected intravenously with either PBS or S2P$_{50}$-siCamk2g NPs at a dose of 1 nmol siRNA per mouse. For acute toxicity studies, treatment with PBS or S2P$_{50}$-siCamk2g NPs was carried out for five consecutive days, with one injection per day. For long-term toxicity studies, treatment with PBS or S2P$_{50}$-siCamk2g NPs was carried out for 4 weeks, with two injections per week. Three days after the last injection, the mice were euthanized, blood was analyzed for the indicated biochemical and hematological end points in the Longwood Small Animal Imaging Facility at Beth Israel Deaconess Medical Center, and sections of organs were stained with H&E in the Rodent Histopathology Core at Harvard Medical School. To assess possible immunological responses to the NPs, female BALB/c mice were injected intravenously with PBS, empty S2P$_{50}$ NPs at the same NP dose as the S2P$_{50}$-siCamk2g NPs, or S2P$_{50}$-siCamk2g NPs at an siRNA dose of 1 nmol per mouse. Twenty-four hours later, serum samples were analyzed by enzyme-linked immunosorbent assay (ELISA) for TNF-α and IL-12 using the corresponding ELISA kits (BioLegend, catalog nos. 430907 and 431601).

Analysis of atherosclerotic lesions

After 8 weeks of WD feeding, *Ldlr*$^{-/-}$ mice were intravenously injected twice a week with PBS, S2P$_{50}$ NPs loaded with control RNA (CtrRNA; 1 nmol of RNA per injection), or S2P$_{50}$ NPs carrying siCamk2g (1 nmol of siRNA per injection) for another 4 weeks, while being maintained on the WD. At the time of harvest, mice were euthanized using isoflurane. Blood was collected by left ventricular puncture, and the vasculature was then perfused with cold PBS. The heart with attached aortic root was either placed in optical cutting temperature (OCT) compound and frozen or fixed in 4% paraformaldehyde and subsequently paraffin embedded. Serial 8- or 6-μm sections of the aortic root were obtained from frozen or fixed/paraffin-embedded samples, respectively. For morphometric analysis, six sections 60 μm apart were stained with Harris' H&E, and total lesion and necrotic core sizes were assessed, as described previously (*12*). For immunofluorescence imaging, sections were blocked with 1% bovine serum albumin for 1 hour, incubated overnight at 4°C with anti-Mac2 (Cedarlane Labs, catalog no. CL8942AP, 1:10,000) or MerTK (R&D Systems, catalog no. AF591, 1:500), rinsed with PBS three times, incubated with fluorescently labeled secondary antibodies for 2 hours, and counterstained with 4′,6-diamidino-2-phenylindole (DAPI). Immunofluorescence images were captured using a Zeiss epifluorescence microscope and analyzed using FIJI software. Picrosirius red (Polysciences, catalog no. 24901A) was used to stain collagen. Collagen cap thickness was quantified from the shoulder regions and the midpoint of every plaque and scored per lesion size (*12*).

Isolation of aortic and splenic cells

Animals were euthanized, and the vasculature was quickly perfused by left ventricular puncture using PBS with heparin (20 U/ml). The aorta was microdissected, taking great care to remove all periaortic fat and adventitia. Aortas and spleen were then harvested under a dissection microscope. Aortas were cut with at least 200 times with dissecting scissors, homogenized, and incubated for 45 min at 37°C in an enzymatic cocktail (1 ml per 10 mg tissue) containing collagenase I (1000 U/ml; Sigma-Aldrich, catalog no. C0130), collagenase XI (400 U/ml; Sigma-Aldrich, catalog no. C7657), hyaluronidase (250 U/ml; Sigma-Aldrich, catalog no. H3506), and deoxyribonuclease I (120 U/ml; Sigma-Aldrich, catalog no. D4527) in an enzymatic digestion buffer containing PBS and 20 mM Hepes. Spleens were harvested and nonenzymatically processed to form a single-cell suspension and then placed through a 70-μm filter. After red blood cell lysis, cells were then stained similar to aortic cell preparations. Tissues were then passed through a 70-μm cell strainer. Red blood cells were lysed from spleen using NH_4Cl. Cells were counted, diluted to 1×10^6 cells per 100 μl, and incubated with antibodies for 2 hours at 4°C. Cells were washed and resuspended in fluorescence-activated cell sorting (FACS) buffer and analyzed using FlowJo software.

Measurement of glucose, cholesterol, complete blood counts, and Ly6C$^{hi/low}$ monocytes

Blood glucose was measured from fasting mice using a glucometer (OneTouch Ultra, LifeScan). Cholesterol was assayed using the Free Cholesterol E kit from Wako (catalog no. 993-02501) according to the manufacturer's protocol. Complete blood cell counts were quantified using a ForCyte Hematology Analyzer (Oxford Science). Blood cells were suspended in FACS staining buffer (PBS containing 2% FBS and 1 mM EDTA) at a density of 1×10^6 cells/100 μl and incubated with Fc block (anti-mouse CD16/32; BioLegend) for 1 hour at 4°C. Cell surface immunostaining was carried out with fluorescent antibodies for 1 hour at 4°C (CD115, 1:100, BioLegend; Ly6C: 1:100, BioLegend). Cells were washed in FACS buffer twice and then resuspended for analysis on a BD FACSCanto II flow cytometer. Data analysis was carried out using FlowJo software.

In situ efferocytosis assay

Acetone-fixed aortic root sections were incubated with TUNEL staining reagents at 37°C for 60 min and then washed three times with PBS. Sections were then blocked with 1% (v/v) bovine serum albumin in PBS for 60 min, incubated overnight at 4°C with anti-Mac2 antibody (1:10,000, Cedarlane), incubated with fluorescently labeled secondary antibodies, and counterstained with DAPI. In situ efferocytosis was scored by counting TUNEL$^+$ nuclei surrounded by or in contact with neighboring Mac2$^+$ macrophages. Free ACs showed nuclear condensation and loss of antibody reactivity and were not in contact with nearby macrophages. Images were captured on a Zeiss epifluorescence microscope and analyzed using FIJI software. Data were plotted as a ratio of associated-to-free cells.

Downloaded from http://stm.sciencemag.org/ at Columbia University Libraries on July 30, 2020

Immunoblotting

Cells were lysed in 2× Laemmli buffer with 50 mM dithiothreitol and boiled at 100°C for 10 min. Lysates were separated on 4 to 20% gradient SDS–polyacrylamide gels and electrotransferred to polyvinylidene difluoride membranes. Membranes were blocked with nonfat dry milk dissolved in tris-buffered saline with 0.1% Tween-20 for 1 hour. Membranes were rinsed and then incubated overnight at 4°C with primary antibodies, which included those for CaMKIIγ (Novus Biologicals, catalog no. NBP2-15685, 1:400), MerTK (R&D Systems, catalog no. AF591, 1:1000), and β-actin [horseradish peroxidase (HRP) conjugate, Cell Signaling Technologies, catalog no. 5125, 1:10,000], and then detected using HRP-conjugated secondary antibodies. Densitometry was performed using FIJI software.

Statistical analysis

All experiments were performed in triplicate unless otherwise stated. Error bars in this study indicate SEM. Statistics were performed using GraphPad Prism 5 software. Normality was determined using D'Agostino-Pearson and/or Shapiro-Wilk normality testing. Unless noted otherwise in the individual figure legends, the data displayed fit a normal distribution. P values for normally distributed data were calculated by either Student's t test (two-tailed) or one-way analysis of variance (ANOVA) with Fisher's least significant difference post hoc analysis when three or more groups were tested. P values for non–normally distributed data were calculated using the Mann-Whitney U test or the Kruskal-Wallis test with an uncorrected Dunn's post hoc analysis. A P value <0.05 was considered statistically significant. Statistical values shown in all figures were according to the following scale: $^*P < 0.05$, $^{**}P < 0.01$, and $^{***}P < 0.001$.

SUPPLEMENTARY MATERIALS

stm.sciencemag.org/cgi/content/full/12/553/eaay1063/DC1

Fig. S1. Synthesis of DSPE-PEG-S2P and its characterization by ^{1}H NMR spectrum.
Fig. S2. Assessment of NP stability.
Fig. S3. Change of NP diameter over time.
Fig. S4. Encapsulation efficiency of siRNA in $S2P_0$ and $S2P_{50}$ NPs.
Fig. S5. NP morphology.
Fig. S6. Serum stability of siRNA-loaded $S2P_{50}$ NPs.
Fig. S7. Silencing of luciferase in HeLa-Luc cells by $S2P_0$-siLuc NPs.
Fig. S8. Effect of $S2P_{50}$-siLuc NPs on cell viability in vitro.
Fig. S9. Apoptosis assays.
Fig. S10. Proliferation assays.
Fig. S11. NP uptake and stabilin-2 expression in macrophages and nonmacrophage cell types.
Fig. S12. Time course of Dy647 fluorescence in whole blood of mice injected with free Dy647-siRNA or Dy647-siRNA in $S2P_0$ and $S2P_{50}$ NPs.
Fig. S13. Gating strategy for aortic macrophages.
Fig. S14. Biodistribution of Alexa 647–conjugated $S2P_0$- and $S2P_{50}$-siCamk2g NPs.
Fig. S15. FACS analysis of fluorescent NPs in splenocytes 24 hours after NP injection into WD-fed *Ldlr*$^{-/-}$ mice.
Fig. S16. Effect of siCamk2g $S2P_{50}$ NPs on macrophage efferocytosis.
Fig. S17. CaMKIIγ silencing with NPs enhances efferocytosis as assessed by flow cytometry.
Fig. S18. CaMKIIγ expression in lesional SMCs and ECs in NP-treated *Ldlr*$^{-/-}$ mice.
Fig. S19. CaMKIIγ expression in splenic macrophages in NP-treated *Ldlr*$^{-/-}$ mice.
Fig. S20. CaMKIIγ expression in liver macrophages in NP-treated *Ldlr*$^{-/-}$ mice.
Fig. S21. Metabolic parameters and blood cell counts of WD-fed *Ldlr*$^{-/-}$ mice treated with PBS or $S2P_{50}$ NPs containing control siRNA or siCamk2g.
Fig. S22. Histological analyses of the major organs in NP-treated *Ldlr*$^{-/-}$ mice.
Fig. S23. Plasma TNF-α and IL-12 concentrations in mice injected with PBS, empty $S2P_{50}$ NPs, or $S2P_{50}$-siCamk2g NPs.
Fig. S24. Summary scheme of the study.

View/request a protocol for this paper from *Bio-protocol*.

REFERENCES AND NOTES

1. K. J. Moore, I. Tabas, Macrophages in the pathogenesis of atherosclerosis. *Cell* **145**, 341–355 (2011).
2. D. Castanotto, J. J. Rossi, The promises and pitfalls of RNA-interference-based therapeutics. *Nature* **457**, 426–433 (2009).
3. K. A. Whitehead, R. Langer, D. G. Anderson, Knocking down barriers: Advances in siRNA delivery. *Nat. Rev. Drug Discov.* **8**, 129–138 (2009).
4. H. Yin, R. L. Kanasty, A. A. Eltoukhy, A. J. Vegas, J. R. Dorkin, D. G. Anderson, Non-viral vectors for gene-based therapy. *Nat. Rev. Genet.* **15**, 541–555 (2014).
5. R. Kanasty, J. R. Dorkin, A. Vegas, D. Anderson, Delivery materials for siRNA therapeutics. *Nat. Mater.* **12**, 967–977 (2013).
6. A. Mullard, FDA approves landmark RNAi drug. *Nat. Rev. Drug Discov.* **17**, 613 (2018).
7. A. M. Flores, J. Ye, K.-U. Jarr, N. Hosseini-Nassab, B. R. Smith, N. J. Leeper, Nanoparticle therapy for vascular diseases. *Arterioscler. Thromb. Vasc. Biol.* **39**, 635–646 (2019).
8. M. Frank-Kamenetsky, A. Grefhorst, N. N. Anderson, T. S. Racie, B. Bramlage, A. Akinc, D. Butler, K. Charisse, R. Dorkin, Y. Fan, C. Gamba-Vitalo, P. Hadwiger, M. Jayaraman, M. John, K. N. Jayaprakash, M. Maier, L. Nechev, K. G. Rajeev, T. Read, I. Röhl, J. Soutschek, P. Tan, J. Wong, G. Wang, T. Zimmermann, A. de Fougerolles, H.-P. Vornlocher, R. Langer, D. G. Anderson, M. Manoharan, V. Koteliansky, J. D. Horton, K. Fitzgerald, Therapeutic RNAi targeting PCSK9 acutely lowers plasma cholesterol in rodents and LDL cholesterol in nonhuman primates. *Proc. Natl. Acad. Sci. U.S.A.* **105**, 11915–11920 (2008).
9. T. S. Zimmermann, A. C. H. Lee, A. Akinc, B. Bramlage, D. Bumcrot, M. N. Fedoruk, J. Harborth, J. A. Heyes, L. B. Jeffs, M. John, A. D. Judge, K. Lam, K. McClintock, L. V. Nechev, L. R. Palmer, T. Racie, I. Röhl, S. Seiffert, S. Shanmugam, V. Sood, J. Soutschek, I. Toudjarska, A. J. Wheat, E. Yaworski, W. Zedalis, V. Koteliansky, M. Manoharan, H.-P. Vornlocher, I. MacLachlan, RNAi-mediated gene silencing in non-human primates. *Nature* **441**, 111–114 (2006).
10. M. Tadin-Strapps, L. B. Peterson, A.-M. Cumiskey, R. L. Rosa, V. H. Mendoza, J. Castro-Perez, O. Puig, L. Zhang, W. R. Strapps, S. Yendluri, L. Andrews, V. Pickering, J. Rice, L. Luo, Z. Chen, S. Tep, B. Ason, E. P. Somers, A. B. Sachs, S. R. Bartz, J. Tian, J. Chin, B. K. Hubbard, K. K. Wong, L. J. Mitnaul, siRNA-induced liver ApoB knockdown lowers serum LDL-cholesterol in a mouse model with human-like serum lipids. *J. Lipid Res.* **52**, 1084–1097 (2011).
11. H. Pan, R. U. Palekar, K. K. Hou, J. Bacon, H. Yan, L. E. Springer, A. Akk, L. Yang, M. J. Miller, C. T. Pham, P. H. Schlesinger, S. A. Wickline, Anti-JNK2 peptide-siRNA nanostructures improve plaque endothelium and reduce thrombotic risk in atherosclerotic mice. *Int. J. Nanomedicine* **13**, 5187–5205 (2018).
12. A. C. Doran, L. Ozcan, B. Cai, Z. Zheng, G. Fredman, C. C. Rymond, B. Dorweiler, J. C. Sluimer, J. Hsieh, G. Kuriakose, A. R. Tall, I. Tabas, CAMKIIγ suppresses an efferocytosis pathway in macrophages and promotes atherosclerotic plaque necrosis. *J. Clin. Invest.* **127**, 4075–4089 (2017).
13. A. V. Finn, M. Nakano, J. Narula, F. D. Kolodgie, R. Virmani, Concept of vulnerable/unstable plaque. *Arterioscler. Thromb. Vasc. Biol.* **30**, 1282–1292 (2010).
14. X. Zhu, Y. Xu, L. M. Solis, W. Tao, L. Wang, C. Behrens, X. Xu, L. Zhao, D. Liu, J. Wu, N. Zhang, I. I. Wistuba, O. C. Farokhzad, B. R. Zetter, J. Shi, Long-circulating siRNA nanoparticles for validating Prohibitin1-targeted non-small cell lung cancer treatment. *Proc. Natl. Acad. Sci. U.S.A.* **112**, 7779–7784 (2015).
15. M. A. Islam, Y. Xu, W. Tao, J. M. Ubellacker, M. Lim, D. Aum, G. Y. Lee, K. Zhou, H. Zope, M. Yu, W. Cao, J. T. Oswald, M. Dinarvand, M. Mahmoudi, R. Langer, P. W. Kantoff, O. C. Farokhzad, B. R. Zetter, J. Shi, Restoration of tumour-growth suppression in vivo via systemic nanoparticle-mediated delivery of PTEN mRNA. *Nat. Biomed. Eng.* **2**, 850–864 (2018).
16. G. Y. Lee, J.-H. Kim, G. T. Oh, B.-H. Lee, I. C. Kwon, I.-S. Kim, Molecular targeting of atherosclerotic plaques by a stabilin-2-specific peptide ligand. *J. Control. Release* **155**, 211–217 (2011).
17. W. Gao, Y. Zhao, X. Li, Y. Sun, M. Cai, W. Cao, Z. Liu, L. Tong, G. Cui, B. Tang, H_2O_2-responsive and plaque-penetrating nanoplatform for mTOR gene silencing with robust anti-atherosclerosis efficacy. *Chem. Sci.* **9**, 439–445 (2018).
18. S.-Y. Park, M.-Y. Jung, H.-J. Kim, S.-J. Lee, S.-Y. Kim, B.-H. Lee, T.-H. Kwon, R.-W. Park, I.-S. Kim, Rapid cell corpse clearance by stabilin-2, a membrane phosphatidylserine receptor. *Cell Death Differ.* **15**, 192–201 (2008).
19. G. Fredman, N. Kamaly, S. Spolitu, J. Milton, D. Ghorpade, R. Chiasson, G. Kuriakose, M. Perretti, O. Farokzhad, I. Tabas, Targeted nanoparticles containing the proresolving peptide Ac2-26 protect against advanced atherosclerosis in hypercholesterolemic mice. *Sci. Transl. Med.* **7**, 275ra220 (2015).
20. N. Kamaly, G. Fredman, M. Subramanian, S. Gadde, A. Pesic, L. Cheung, Z. A. Fayad, R. Langer, I. Tabas, O. C. Farokhzad, Development and in vivo efficacy of targeted polymeric inflammation-resolving nanoparticles. *Proc. Natl. Acad. Sci. U.S.A.* **110**, 6506–6511 (2013).
21. M. Lameijer, T. Binderup, M. M. T. van Leent, M. L. Senders, F. Fay, J. Malkus, B. L. Sanchez-Gaytan, A. J. P. Teunissen, N. Karakatsanis, P. Robson, X. Zhou, Y. Ye, G. Wojtkiewicz, J. Tang,

Downloaded from http://stm.sciencemag.org/ at Columbia University Libraries on July 30, 2020

T. T. P. Seijkens, J. Kroon, E. S. G. Stroes, A. Kjaer, J. Ochando, T. Reiner, C. Pérez-Medina, C. Calcagno, E. A. Fisher, B. Zhang, R. E. Temel, F. K. Swirski, M. Nahrendorf, Z. A. Fayad, E. Lutgens, W. J. M. Mulder, R. Duivenvoorden, Efficacy and safety assessment of a TRAF6-targeted nanoimmunotherapy in atherosclerotic mice and non-human primates. *Nat. Biomed. Eng.* **2**, 279–292 (2018).
22. S. D. Funk, A. Yurdagul Jr., J. M. Green, K. A. Jhaveri, M. A. Schwartz, A. W. Orr, Matrix-specific protein kinase A signaling regulates p21-activated kinase activation by flow in endothelial cells. *Circ. Res.* **106**, 1394–1403 (2010).
23. A. W. Orr, R. Stockton, M. B. Simmers, J. M. Sanders, I. J. Sarembock, B. R. Blackman, M. A. Schwartz, Matrix-specific p21-activated kinase activation regulates vascular permeability in atherogenesis. *J. Cell Biol.* **176**, 719–727 (2007).
24. X. Xu, K. Xie, X.-Q. Zhang, E. M. Pridgen, G. Y. Park, D. S. Cui, J. Shi, J. Wu, P. W. Kantoff, S. J. Lippard, R. Langer, G. C. Walker, O. C. Farokhzad, Enhancing tumor cell response to chemotherapy through nanoparticle-mediated codelivery of siRNA and cisplatin prodrug. *Proc. Natl. Acad. Sci. U.S.A.* **110**, 18638–18643 (2013).
25. G. Sahay, W. Querbes, C. Alabi, A. Eltoukhy, S. Sarkar, C. Zurenko, E. Karagiannis, K. Love, D. Chen, R. Zoncu, Y. Buganim, A. Schroeder, R. Langer, D. G. Anderson, Efficiency of siRNA delivery by lipid nanoparticles is limited by endocytic recycling. *Nat. Biotechnol.* **31**, 653–658 (2013).
26. J. Gilleron, W. Querbes, A. Zeigerer, A. Borodovsky, G. Marsico, U. Schubert, K. Manygoats, S. Seifert, C. Andree, M. Stöter, H. Epstein-Barash, L. Zhang, V. Koteliansky, K. Fitzgerald, E. Fava, M. Bickle, Y. Kalaidzidis, A. Akinc, M. Maier, M. Zerial, Image-based analysis of lipid nanoparticle–mediated siRNA delivery, intracellular trafficking and endosomal escape. *Nat. Biotechnol.* **31**, 638–646 (2013).
27. C. V. Pecot, G. A. Calin, R. L. Coleman, G. Lopez-Berestein, A. K. Sood, RNA interference in the clinic: Challenges and future directions. *Nat. Rev. Cancer* **11**, 59–67 (2011).
28. J. Soutschek, A. Akinc, B. Bramlage, K. Charisse, R. Constien, M. Donoghue, S. Elbashir, A. Geick, P. Hadwiger, J. Harborth, M. John, V. Kesavan, G. Lavine, R. K. Pandey, T. Racie, K. G. Rajeev, I. Röhl, I. Toudjarska, G. Wang, S. Wuschko, D. Bumcrot, V. Koteliansky, S. Limmer, M. Manoharan, H.-P. Vornlocher, Therapeutic silencing of an endogenous gene by systemic administration of modified siRNAs. *Nature* **432**, 173–178 (2004).
29. S. Katsuki, T. Matoba, S. Nakashiro, K. Sato, J.-i. Koga, K. Nakano, Y. Nakano, S. Egusa, K. Sunagawa, K. Egashira, Nanoparticle-mediated delivery of pitavastatin inhibits atherosclerotic plaque destabilization/rupture in mice by regulating the recruitment of inflammatory monocytes. *Circulation* **129**, 896–906 (2014).
30. R. Duivenvoorden, J. Tang, D. P. Cormode, A. J. Mieszawska, D. Izquierdo-Garcia, C. Ozcan, M. J. Otten, N. Zaidi, M. E. Lobatto, S. M. van Rijs, B. Priem, E. L. Kuan, C. Martel, B. Hewing, H. Sager, M. Nahrendorf, G. J. Randolph, E. S. G. Stroes, V. Fuster, E. A. Fisher, Z. A. Fayad, W. J. M. Mulder, A statin-loaded reconstituted high-density lipoprotein nanoparticle inhibits atherosclerotic plaque inflammation. *Nat. Commun.* **5**, 3065 (2014).
31. J. Tang, M. E. Lobatto, L. Hassing, S. van der Staay, S. M. van Rijs, C. Calcagno, M. S. Braza, S. Baxter, F. Fay, B. L. Sanchez-Gaytan, R. Duivenvoorden, H. Sager, Y. M. Astudillo, W. Leong, S. Ramachandran, G. Storm, C. Pérez-Medina, T. Reiner, D. P. Cormode, G. J. Strijkers, E. S. G. Stroes, F. K. Swirski, M. Nahrendorf, E. A. Fisher, Z. A. Fayad, W. J. M. Mulder, Inhibiting macrophage proliferation suppresses atherosclerotic plaque inflammation. *Sci. Adv.* **1**, e1400223 (2015).
32. M. Yu, J. Amengual, A. Menon, N. Kamaly, F. Zhou, X. Xu, P. E. Saw, S.-J. Lee, K. Si, C. A. Ortega, W. I. Choi, I.-H. Lee, Y. Bdour, J. Shi, M. Mahmoudi, S. Jon, E. A. Fisher, O. C. Farokhzad, Targeted nanotherapeutics encapsulating liver X receptor agonist GW3965 enhance antiatherogenic effects without adverse effects on hepatic lipid metabolism in *Ldlr*$^{-/-}$ Mice. *Adv.Healthc. Mater.* **6**, 1700313 (2017).
33. D. R. Lewis, L. K. Petersen, A. W. York, K. R. Zablocki, L. B. Joseph, V. Kholodovych, R. K. Prud'homme, K. E. Uhrich, P. V. Moghe, Sugar-based amphiphilic nanoparticles arrest atherosclerosis in vivo. *Proc. Natl. Acad. Sci. U.S.A.* **112**, 2693–2698 (2015).
34. S. Nakashiro, T. Matoba, R. Umezu, J.-I. Koga, M. Tokutome, S. Katsuki, K. Nakano, K. Sunagawa, K. Egashira, Pioglitazone-incorporated nanoparticles prevent plaque destabilization and rupture by regulating monocyte/macrophage differentiation in *ApoE*$^{-/-}$ mice. *Arterioscler. Thromb. Vasc. Biol.* **36**, 491–500 (2016).
35. T. T. P. Seijkens, C. M. van Tiel, P. J. H. Kusters, D. Atzler, O. Soehnlein, B. Zarzycka, S. A. B. M. Aarts, M. Lameijer, M. J. Gijbels, L. Beckers, M. den Toom, B. Slütter, J. Kuiper, J. Duchene, M. Aslani, R. T. A. Megens, C. van 't Veer, G. Kooij, R. Schrijver, M. A. Hoeksema, L. Boon, F. Fay, J. Tang, S. Baxter, A. Jongejan, P. D. Moerland, G. Vriend, B. Bleijlevens, E. A. Fisher, R. Duivenvoorden, N. Gerdes, M. P. J. de Winther, G. A. Nicolaes, W. J. M. Mulder, C. Weber, E. Lutgens, Targeting CD40-induced TRAF6 signaling in macrophages reduces atherosclerosis. *J. Am. Coll. Cardiol.* **71**, 527–542 (2018).
36. J. R. McCarthy, E. Korngold, R. Weissleder, F. A. Jaffer, A light-activated theranostic nanoagent for targeted macrophage ablation in inflammatory atherosclerosis. *Small* **6**, 2041–2049 (2010).
37. H. Kosuge, S. P. Sherlock, T. Kitagawa, R. Dash, J. T. Robinson, H. Dai, M. V. McConnell, Near infrared imaging and photothermal ablation of vascular inflammation using single-walled carbon nanotubes. *J. Am. Heart Assoc.* **1**, e002568 (2012).
38. F. Leuschner, P. Dutta, R. Gorbatov, T. I. Novobrantseva, J. S. Donahoe, G. Courties, K. M. Lee, J. I. Kim, J. F. Markmann, B. Marinelli, P. Panizzi, W. W. Lee, Y. Iwamoto, S. Milstein, H. Epstein-Barash, W. Cantley, J. Wong, V. Cortez-Retamozo, A. Newton, K. Love, P. Libby, M. J. Pittet, F. K. Swirski, V. Koteliansky, R. Langer, R. Weissleder, D. G. Anderson, M. Nahrendorf, Therapeutic siRNA silencing in inflammatory monocytes in mice. *Nat. Biotechnol.* **29**, 1005–1010 (2011).
39. X. Xu, P. E. Saw, W. Tao, Y. Li, X. Ji, M. Yu, M. Mahmoudi, J. Rasmussen, D. Ayyash, Y. Zhou, O. C. Farokhzad, J. Shi, Tumor microenvironment-responsive multistaged nanoplatform for systemic RNAi and cancer therapy. *Nano Lett.* **17**, 4427–4435 (2017).
40. X. Xu, J. Wu, Y. Liu, P. E. Saw, W. Tao, M. Yu, H. Zope, M. Si, A. Victorious, J. Rasmussen, D. Ayyash, O. C. Farokhzad, J. Shi, Multifunctional envelope-type siRNA delivery nanoparticle platform for prostate cancer therapy. *ACS Nano* **11**, 2618–2627 (2017).
41. X. Zhu, W. Tao, D. Liu, J. Wu, Z. Guo, X. Ji, Z. Bharwani, L. Zhao, X. Zhao, O. C. Farokhzad, J. Shi, Surface De-PEGylation controls nanoparticle-mediated siRNA delivery *in vitro* and *in vivo*. *Theranostics* **7**, 1990–2002 (2017).
42. N. Kong, W. Tao, X. Ling, J. Wang, Y. Xiao, S. Shi, X. Ji, A. Shajii, S. T. Gan, N. Y. Kim, D. G. Duda, T. Xie, O. C. Farokhzad, J. Shi, Synthetic mRNA nanoparticle-mediated restoration of p53 tumor suppressor sensitizes *p53*-deficient cancers to mTOR inhibition. *Sci. Transl. Med.* **11**, eaaw1565 (2019).
43. S. Barua, S. Mitragotri, Challenges associated with penetration of nanoparticles across cell and tissue barriers: A review of current status and future prospects. *Nano Today* **9**, 223–243 (2014).
44. N. Kamaly, G. Fredman, J. J. R. Fojas, M. Subramanian, W. I. Choi, K. Zepeda, C. Vilos, M. Yu, S. Gadde, J. Wu, J. Milton, R. Carvalho Leitao, L. Rosa Fernandes, M. Hasan, H. Gao, V. Nguyen, J. Harris, I. Tabas, O. C. Farokhzad, Targeted interleukin-10 nanotherapeutics developed with a microfluidic chip enhance resolution of inflammation in advanced atherosclerosis. *ACS Nano* **10**, 5280–5292 (2016).
45. Z. Mallat, Macrophages. *Arterioscler. Thromb. Vasc. Biol.* **37**, e92–e98 (2017).
46. P. M. Ridker, B. M. Everett, T. Thuren, J. G. MacFadyen, W. H. Chang, C. Ballantyne, F. Fonseca, J. Nicolau, W. Koenig, S. D. Anker, J. J. P. Kastelein, J. H. Cornel, P. Pais, D. Pella, J. Genest, R. Cifkova, A. Lorenzatti, T. Forster, Z. Kobalava, L. Vida-Simiti, M. Flather, H. Shimokawa, H. Ogawa, M. Dellborg, P. R. F. Rossi, R. P. T. Troquay, P. Libby, R. J. Glynn; CANTOS Trial Group, Antiinflammatory therapy with canakinumab for atherosclerotic disease. *N. Engl. J. Med.* **377**, 1119–1131 (2017).

Acknowledgments: We thank the Dana-Farber/Harvard Cancer Center in Boston, MA, for the use of the Rodent Histopathology Core, which provided H&E staining service. We also thank the Confocal and Specialized Microscopy Core at Columbia University's Irving Cancer Research Center for the assistance with lesional imaging. We also thank G. Kuriakose very much for technical contributions related to the atherosclerosis studies. **Funding:** This work was supported by NIH grants HL145131 (A.Y.), HL127464 (O.C.F., I.T., and J.S.), HL132412 (I.T.), and HL145228 (I.T.); a Liver Scholar Award (X.W.); an American Heart Association (AHA) Fellow to Faculty Award (A.C.D.); and Brigham and Women's Hospital Khoury Innovation award no.122829 (W.T.). **Author contributions:** W.T., A.Y.J., O.C.F., I.T., and J.S. conceived, designed, and directed the research; W.T. and W.L. designed, engineered, and optimized the targeted NP technologies used in this publication; W.T., N.K., and C.F. performed the characterization, late endosomal escape efficiency, silencing of luciferase, and in vitro and in vivo toxicity studies of the developed NPs. W.T. and A.Y. conducted the biodistribution, in vitro and in vivo targeting of macrophages, and atherosclerotic plaque studies. X.W., A.C.D., J.W., and M.A.I. provided technical support and edited the manuscript. W.T. and A.Y. wrote the manuscript, which was subsequently edited by O.C.F., I.T., and J.S. **Competing interests:** In compliance with the Brigham and Women's Hospital and Harvard Medical School institutional guidelines, O.C.F. discloses his financial interest in Selecta Biosciences, Tarveda Therapeutics, and Seer. **Data and materials availability:** All data associated with this study are present in the paper or the Supplementary Materials.

Submitted 20 May 2019
Resubmitted 26 February 2020
Accepted 15 June 2020
Published 22 July 2020
10.1126/scitranslmed.aay1063

Citation: W. Tao, A. Yurdagul Jr., N. Kong, W. Li, X. Wang, A. C. Doran, C. Feng, J. Wang, M. A. Islam, O. C. Farokhzad, I. Tabas, J. Shi, siRNA nanoparticles targeting CaMKIIγ in lesional macrophages improve atherosclerotic plaque stability in mice. *Sci. Transl. Med.* **12**, eaay1063 (2020).

Downloaded from http://stm.sciencemag.org/ at Columbia University Libraries on July 30, 2020

Science Translational Medicine

siRNA nanoparticles targeting CaMKIIγ in lesional macrophages improve atherosclerotic plaque stability in mice

Wei Tao, Arif Yurdagul, Jr., Na Kong, Wenliang Li, Xiaobo Wang, Amanda C. Doran, Chan Feng, Junqing Wang, Mohammad Ariful Islam, Omid C. Farokhzad, Ira Tabas and Jinjun Shi

Sci Transl Med **12**, eaay1063.
DOI: 10.1126/scitranslmed.aay1063

Perturbing plaque macrophages

Macrophages in atherosclerotic lesions promote inflammation and plaque progression and are an attractive therapeutic target. Here, Tao *et al.* used nanoparticles to inhibit pro-atherogenic macrophages by siRNA targeting Ca^{2+}/calmodulin-dependent protein kinase γ. Nanoparticle treatment induced phagocytosis of apoptotic cells in plaques and promoted plaque stability, reducing necrotic area and increasing fibrous cap thickness in a mouse model of atherosclerosis. This study establishes proof of concept for siRNA nanoparticles targeting lesional macrophages as a treatment for atherosclerosis.

ARTICLE TOOLS http://stm.sciencemag.org/content/12/553/eaay1063

SUPPLEMENTARY MATERIALS http://stm.sciencemag.org/content/suppl/2020/07/20/12.553.eaay1063.DC1

RELATED CONTENT
http://stm.sciencemag.org/content/scitransmed/11/517/eaax0481.full
http://stm.sciencemag.org/content/scitransmed/7/275/275ra20.full
http://stm.sciencemag.org/content/scitransmed/5/196/196ra100.full
http://stm.sciencemag.org/content/scitransmed/6/239/239sr1.full

REFERENCES This article cites 46 articles, 16 of which you can access for free
http://stm.sciencemag.org/content/12/553/eaay1063#BIBL

PERMISSIONS http://www.sciencemag.org/help/reprints-and-permissions

Use of this article is subject to the Terms of Service

Science Translational Medicine (ISSN 1946-6242) is published by the American Association for the Advancement of Science, 1200 New York Avenue NW, Washington, DC 20005. The title *Science Translational Medicine* is a registered trademark of AAAS.

Copyright © 2020 The Authors, some rights reserved; exclusive licensee American Association for the Advancement of Science. No claim to original U.S. Government Works

Downloaded from http://stm.sciencemag.org/ at Columbia University Libraries on July 30, 2020